Asian Journal of Chemistry; Vol. 38, No. 6 (2026), 1599-1612
ASIAN JOURNAL OF CHEMISTRY
https://doi.org/10.14233/ajchem.2026.35845

Comparative Evaluation of the Adsorptive Affinity of Zn-H_2BDC/H_3BTC Framework for Cationic and Anionic Dyes: Equilibrium, Kinetic and Thermodynamic Approach

SAMUEL UKACHUKU[1,2,*] and EZEKIEL D. DIKIO[2]

[1]Department of Pure and Industrial Chemistry, University of Africa, Toru-Orua, Bayelsa State, Nigeria
[2]Department of Chemical Sciences, Niger Delta University, Wilberforce Island, Bayelsa State, Nigeria

*Corresponding author: E-mail: samuel.ukachuku@uat.edu.ng

Received: 3 March 2026 *Accepted*: 16 May 2026 *Published online*: 31 May 2026 AJC-22387

This study reports the adsorption selectivity of the mixed-linker metal-organic framework Zn-H_2BDC/H_3BTC toward cationic and anionic dyes represented by malachite green (MG) and acid orange 7 (AO7), respectively. The MOF was synthesized *via* a solvothermal method and characterized using FTIR, PXRD and TGA/DTG analyses, which confirmed the successful formation of the framework, high crystallinity and adequate thermal stability for wastewater treatment applications. Batch adsorption experiments were performed by varying initial dye concentration, contact time, pH and temperature. The adsorption capacity increased with increasing dye concentration, while AO7 adsorption was favoured under acidic conditions and reached equilibrium within 60 min, whereas MG adsorption increased gradually under alkaline conditions. Equilibrium studies showed that both Langmuir and Freundlich isotherm models adequately described the adsorption process, indicating the coexistence of monolayer and heterogeneous adsorption mechanisms. The Langmuir maximum adsorption capacity (Q_m) for AO7 (1.848 mg/g) was higher than that for MG (1.469 mg/g), confirming the greater adsorption affinity of Zn-H_2BDC/H_3BTC toward the anionic dye. Elovich isotherm parameters, including Elovich constant (K_E), further indicated higher adsorption affinity and faster uptake of AO7 relative to MG. Kinetic studies revealed that pseudo-second-order kinetics governed AO7 adsorption, whereas intraparticle diffusion significantly influenced MG uptake. Thermodynamic analysis demonstrated that the adsorption processes were spontaneous, exothermic and predominantly controlled by weak physisorption interactions. The results demonstrate that Zn-H_2BDC/H_3BTC possesses selective adsorption behaviour with stronger affinity toward AO7 and may serve as a promising adsorbent for dye-contaminated wastewater treatment.

Keywords: Adsorption, Metal-organic frameworks, Malachite green, Acid orange 7.

INTRODUCTION

Dyes constitute a large class of organic compounds widely used for colour impartation in industries such as textiles, inks, paints, cosmetics, pharmaceuticals, leather, plastics, paper and food processing [1,2]. Their extensive industrial application generates large volumes of coloured effluents that require proper treatment prior to discharge. It has been reported that nearly 700,000 tons of approximately 100,000 different dyes are consumed annually by the textile industry alone [3], contributing significantly to environmental pollution of receiving water bodies [4-7]. Many synthetic dyes exhibit high chemical stability and resistance to biodegradation, resulting in their persistence in aquatic environments. Furthermore, the presence of polyaromatic structures in dye molecules enhances their toxic, mutagenic and carcinogenic potential and promotes their accumulation in sediments and soils [6]. Consequently, dye-contaminated wastewater poses serious environmental and ecological concerns, making the removal of dyes from industrial effluents an important objective in wastewater treatment and environmental management [6].

Treatment of dye-containing effluents remains a major global environmental challenge due to the large volumes of wastewater generated and the complex mixture of contaminants present in industrial discharges [8]. Dye effluents commonly contain various dyes, auxiliary agents, additives and processing chemicals, which complicate wastewater treatment. The conventional treatment methods such as biological treatment, coagulation/flocculation, ozonation, membrane filtration and photocatalytic processes [3,6,7] often suffer from limitations related to operational efficiency, selectivity and cost-effectiveness [9]. Among the available approaches, adsorption has

emerged as one of the most efficient and economically viable techniques due to its simplicity, high removal efficiency and potential for regeneration and reuse of adsorbents [9].

Metal-organic frameworks (MOFs), first introduced over two decades ago [10-12], have attracted considerable attention as advanced adsorbent materials owing to their exceptional porosity, tunable structures and high surface areas [10,13]. MOFs are crystalline porous materials composed of metal ions or clusters coordinated with organic ligands to form extended three-dimensional frameworks [10]. Their structural versatility and adsorption capability have enabled diverse applications, including gas storage [14], heavy metal removal [15], pollutant remediation [16,17], dye adsorption [18], drug delivery [19, 20] and catalysis [21]. Several studies have demonstrated the efficient removal of dyes such as methyl orange [22], aniline blue [23], malachite green [24], methylene blue [13,23], Congo red [25] orange II [23], *etc*. using MOF-based adsorbents.

In present study, a pristine zinc-based MOF containing mixed carboxylate linkers, terephthalate and trimesate anions, was investigated for the adsorption of cationic and anionic dyes. The use of mixed-linker MOFs aligns with recent advances in MOF design aimed at improving structural stability, porosity and adsorption performance [26-31]. Acid orange 7 (AO7) and malachite green (MG) were selected as representative anionic and cationic dyes, respectively, to evaluate the adsorption affinity of the synthesized MOF toward different ionic dye species. The adsorption behaviour was analysed using equilibrium, kinetic and thermodynamic models to understand the interaction mechanisms between the dyes and MOF surface. Although electrostatic attraction is expected to be the dominant adsorption mechanism, additional interactions such as π–π stacking and donor–acceptor interactions between aromatic structures of the dyes and MOF framework may also contribute to adsorption [23]. The findings of this study may provide useful insights into the selective removal of ionic dyes from wastewater using MOF-based adsorbents.

EXPERIMENTAL

The analytical grade reagents *viz*. zinc nitrate hexahydrate ($Zn(NO_3)_2 \cdot 6H_2O$, m.w. 297.49 g/mol), supplied by Aladdin Biological Technology Co., Ltd.; benzene-1,4-dicarboxylic acid (terephthalic acid) and benzene-1,3,5-tricarboxylic acid (trimesic acid), both obtained from Merck KGaA. Oxalate-based malachite green (MG), used as representative cationic dye, was procured from Kem Light Laboratories Pvt. Ltd., while acid orange 7 (AO7), employed as the representative anionic dye, was purchased from BioCrick Bio Tech. Sterile distilled water was used for the preparation of all dye solutions and experimental studies.

Characterization: FT-IR spectra of the as-synthesised Zn-H_2BDC/H_3BTC MOF were recorded using a Perkin-Elmer Spectrum 400 FT-IR/NIR spectrophotometer over the range of 4000-400 cm^{-1} at a resolution of 4 cm^{-1} to identify the functional groups present in the material. Thermal stability was evaluated using a TGA 4000 thermogravimetric analyzer under nitrogen atmosphere from ambient temperature to 1200 ºC at a heating rate of 10 ºC/min. Powder X-ray diffraction (PXRD) patterns were obtained using a D8 Advance diffractometer manufactured by Bruker AXS with Cu*K*α radiation over a 2θ range of 5-90º to determine the crystallinity and phase structure of the synthesized MOF.

Synthesis: Zn-H_2BDC/H_3BTC MOF was synthesized by refluxing a mixture of zinc nitrate (20.82 g, 0.07 mol), terephthalic acid (5.81 g, 0.035 mol) and trimesic acid (7.35 g, 0.035 mol) in 100 mL of N,N-dimethylformamide (DMF) at 140 ºC for 7 h under continuous magnetic stirring. After completion of the reaction, the resulting crystals were separated by decantation and filtration, washed thoroughly with methanol to remove residual solvent molecules and collected by centrifugation (**Scheme-I**). The obtained Zn-H_2BDC/H_3BTC MOF colourless crystals were dried at room temperature and stored for further characterization and adsorption studies.

Batch adsorption studies: A stock solution (100 mg/L) of each dye, malachite green (MG) and acid orange 7 (AO7), was prepared separately by dissolving 0.1 g of dye in distilled water and diluting to 1 L in a volumetric flask. Adsorption experiments were carried out by mixing 0.1 g of Zn-H_2BDC/H_3BTC MOF with 20 mL dye solutions of varying concentrations (2-18 mg/L) in Erlenmeyer flasks, followed by agitation at 100 rpm using an orbital shaker (SHK-O1750, Bioevopeak, China) for 1 h. After adsorption, the suspensions were centrifuged at 2000 rpm for 5 min to obtain clear supernatants. The equilibrium dye concentrations were determined using a double-beam UV-visible spectrophotometer (SP-IUV, Infitek Bioindustry Co. Ltd., China) at the maximum absorption wavelengths (λ_{max}) of 617 nm for MG and 485 nm for AO7. The adsorption capacity (Q_e), representing the amount of dye adsorbed per gram of Zn-H_2BDC/H_3BTC, was calculated using the standard adsorption equation:

$$Q_e = \frac{(C_o - C_t)\,v}{w} \quad (1)$$

where C_o and C_t represent the initial and equilibrium dye concentrations (mg/L); W is the mass of adsorbent used (g) and V is the volume of dye solution (L).

Effect of contact time: The effect of contact time on dye adsorption was investigated over a period of 30-150 min using 0.1 g of Zn-H_2BDC/ H_3BTC and 20 mL of 10 mg/L dye solution in an Erlenmeyer flask. The mixtures were agitated at 100 rpm using an orbital shaker while maintaining constant temperature and pH conditions. After each adsorption interval, the suspensions were centrifuged at 2000 rpm for 5 min and the residual dye concentrations in the supernatants were determined using a UV-visible spectrophotometer.

The amount of dye adsorbed per gram of Zn-H_2BDC/ H_3BTC at any given time, denoted as adsorption capacity (Q_t), was calculated using the following equation:

$$Q_t = \frac{(C_o - C_e)\,v}{w} \quad (6)$$

where C_o and C_t, represent the initial dye concentration and dye concentration at time t (mg/L), respectively; W is the mass of adsorbent used (g) and V is the volume of dye solution (L).

Effect of pH: The effect of pH on dye adsorption was investigated using 0.1 g of Zn-H_2BDC/H_3BTC and 20 mL of 10 mg/L dye solution with pH values adjusted between 3 and 10 using 0.1 M HCl or 0.1 M NaOH solutions. The mixtures

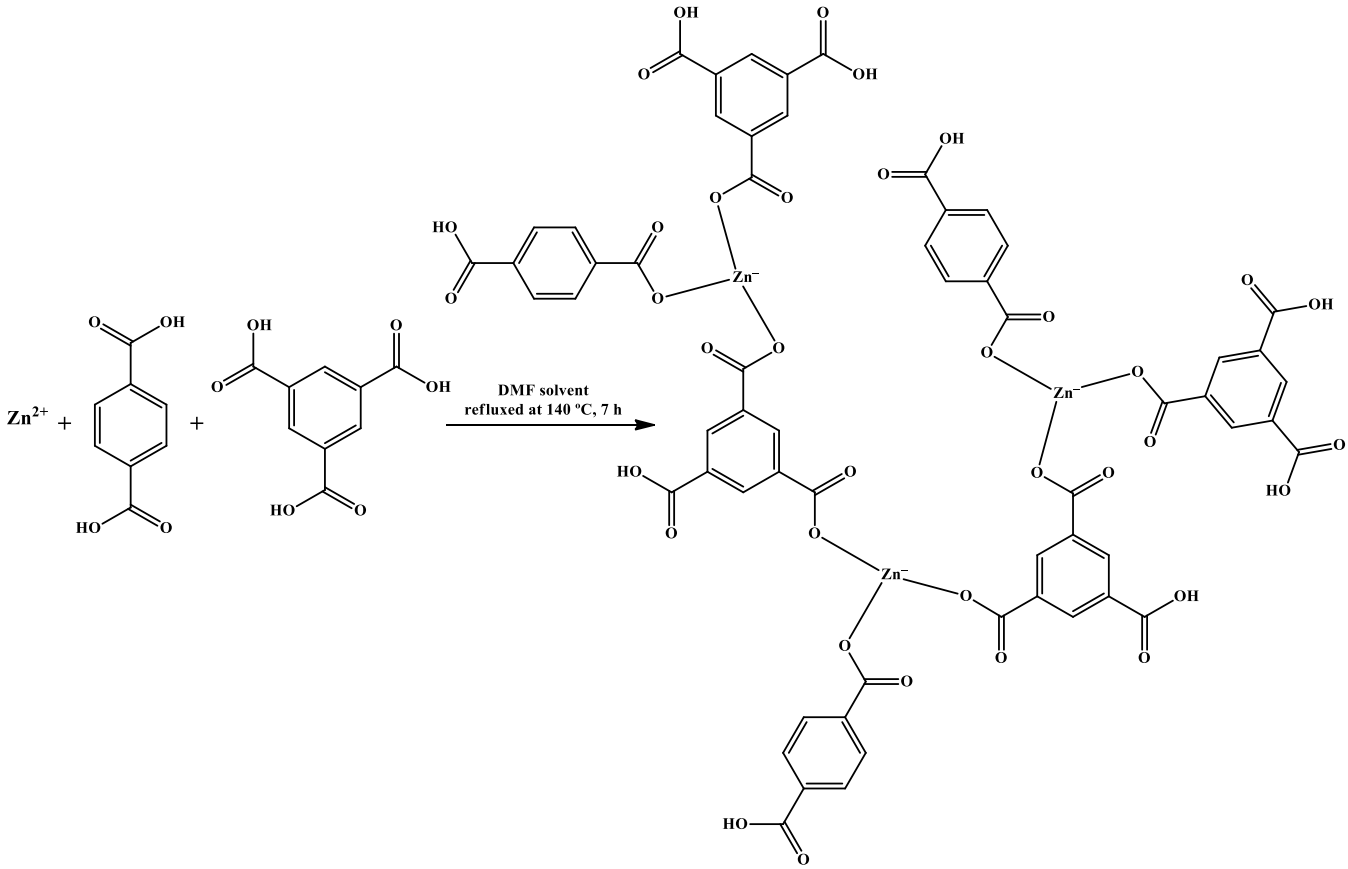

Scheme-I: Synthetic route of mixed-linker metal-organic framework Zn-H_2BDC/H_3BTC

were agitated in Erlenmeyer flasks for 60 min using an orbital shaker, followed by centrifugation at 2000 rpm for 5 min. The residual dye concentrations in the supernatants were determined using a UV-visible spectrophotometer.

Effect of temperature: The effect of temperature on adsorption was studied over the range of 313-333 K using 0.1 g of Zn-H_2BDC/H_3BTC and 20 mL of 10 mg/L dye solution. The experiments were conducted using a temperature-controlled hotplate magnetic stirrer, while the solution temperature was monitored with a mercury thermometer. The mixtures were stirred at 50 rpm for 60 min, centrifuged at 2000 rpm for 5 min and analysed using a UV-visible spectrophotometer to determine the residual dye concentration.

RESULTS AND DISCUSSION

FTIR analysis: The FT-IR spectrum of Zn-H_2BDC/H_3BTC (Fig. 1) confirms the successful formation of the MOF structure. The absorption bands observed in the region 3100-2800 cm^{-1} are attributed to C-H stretching vibrations of aromatic benzene rings and residual DMF molecules trapped within the framework pores. The absence of characteristic carboxylic acid C=O stretching bands in the region 1723-1680 cm^{-1} indicates effective coordination between the organic linkers and Zn metal centres through deprotonation of the carboxylic acid groups. The peaks appearing at 1620, 1573, 1431 and 1359 cm^{-1} correspond to the asymmetric and symmetric stretching vibrations of coordinated carboxylate groups, confirming the

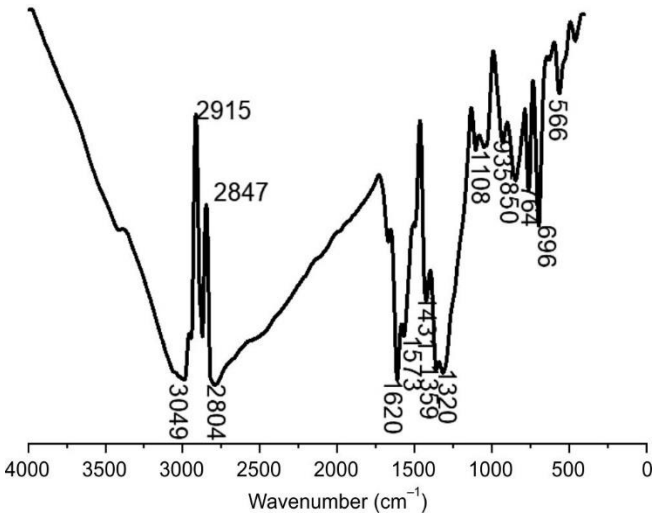

Fig. 1. FTIR spectrum of Zn-H_2BDC/H_3BTC

formation of metal-carboxylate linkages. The bands around 1110-1100 cm^{-1} are assigned to C-O stretching vibrations associated with the C-O-Zn coordination environment. In addition, the bands observed between 935 and 696 cm^{-1} are attributed to in-plane and out-of-plane bending vibrations of aromatic C-H, C-C and C=C bonds, while the band at 566 cm^{-1} corresponds to Zn-O stretching vibrations, further supporting the successful coordination of Zn ions within the MOF framework [32-39].

PXRD analysis: The PXRD patterns of Zn-H_2BDC/H_3BTC was recorded to evaluate the crystallinity and phase structure of the synthesized MOF and is shown in Fig. 2. The diffractogram exhibited distinct and sharp diffraction peaks, confirming the crystalline nature of the material. The percentage crystallinity and amorphous content were determined using XPowderX software (2023 version). The average crystallite size of Zn-H_2BDC/H_3BTC was estimated using the Scherrer's equation given below:

$$D = \frac{K\lambda}{\beta \cos\theta} \quad (14)$$

where D is the crystallite's size in nanometer; K is the Scherrer constant, ranging between 0.89 to 9.4; β is full width at half maximum (FWHM), that is, the width of the XRD peak at exactly halfway of the entire peak height.

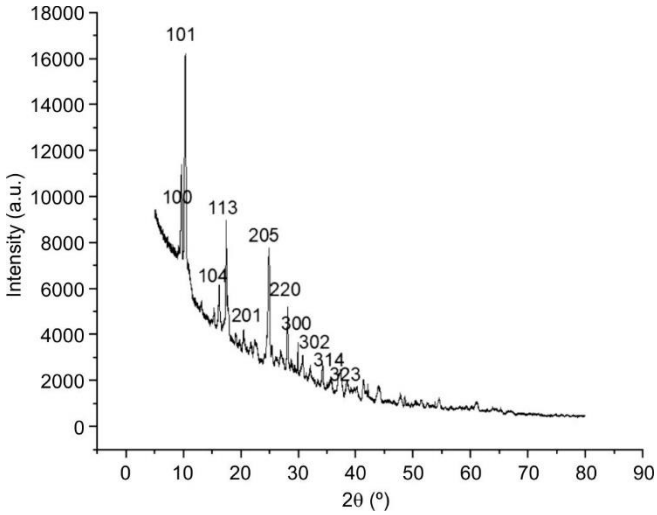

Fig. 2. PXRD diffractogram of Zn-H_2BDC/H_3BTC

The PXRD diffractogram of Zn-H_2BDC/H_3BTC exhibited several well-defined diffraction peaks, with the most intense reflections observed at 2θ values of 9.5º, 10.1º, 15.9º, 17.1º, 24.4º, 27.5º and 29.2º, corresponding to the crystallographic planes (100), (101), (104), (113), (205), (220) and (300), respectively, of a tetragonal crystal system. The presence of sharp and intense diffraction peaks confirms the crystalline nature of the synthesized MOF. The percentage crystallinity and amorphous content were calculated to be 76% and 24%, respectively, indicating predominant crystalline character. The average crystallite size was found to be 22.69 nm.

Thermal studies: The results of the thermogravimetric (TGA) and differential thermogravimetric (DTG) analysis of the as-synthesised Zn-H_2BDC/H_3BTC MOF are shown in Fig. 3.

The TGA of Zn-H_2BDC/H_3BTC MOF revealed four major weight-loss regions, indicating successive decomposition stages of the MOF framework. The initial weight loss (12%) observed between 41-242 ºC is attributed to the removal of physically and chemically trapped solvent molecules within the pores of the framework. The second decomposition stage, occurring between 242-375 ºC, showed a 26% weight loss and is associated with the removal of coordinated solvents, decomposition of residual organic impurities and partial degradation of the MOF structure accompanied by ZnO formation. The third stage (375-575 ºC) exhibited a 28% weight loss due to further decomposition of the organic linkers and structural collapse of the framework [35]. The final decomposition region between 575-1041 ºC resulted in an additional 27% weight loss, likely due to the continued degradation of residual zinc-containing species. The total weight loss recorded was 93%.

The DTG curve displayed five endothermic peaks at 95, 352, 441, 508 and 809 ºC corresponding to phase transitions and decomposition events, while two prominent exothermic peaks at 242 and 575 ºC were associated with framework decomposition and ZnO formation [40]. Although the high weight loss indicates limited thermal stability at high temperatures, the MOF remained relatively stable below 41 ºC, suggesting its suitability for adsorption applications under typical wastewater treatment conditions.

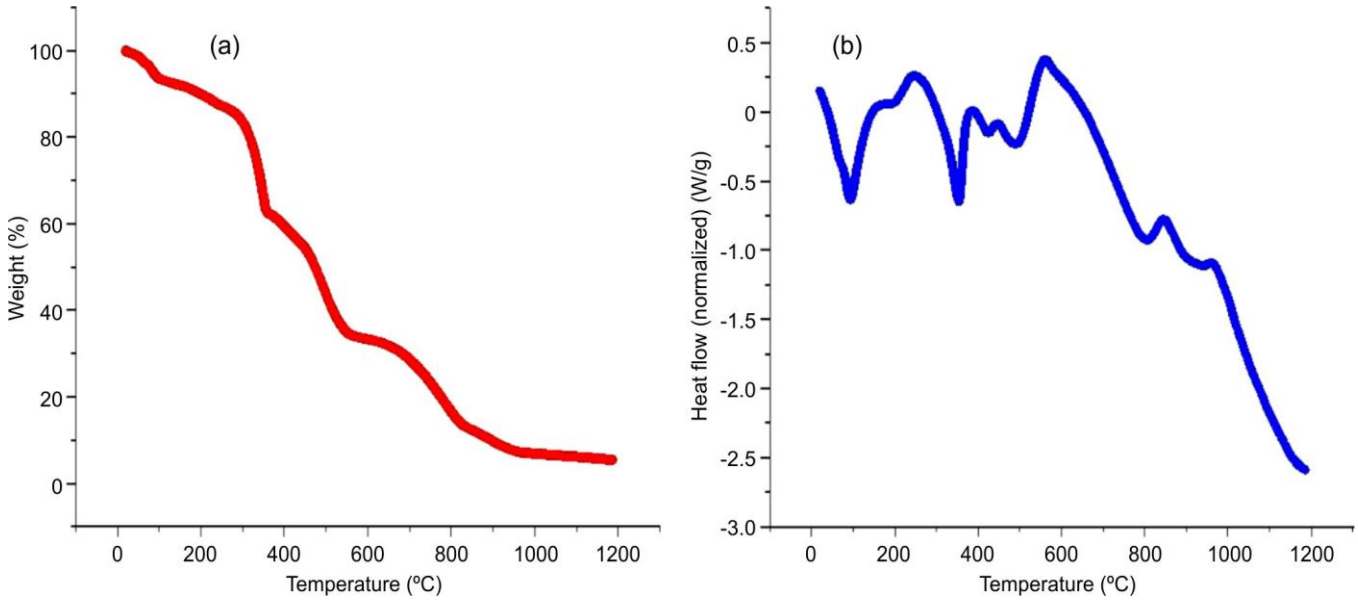

Fig. 3. Thermogravimetric (TG) (a) and derivative thermogravimetric (DTG) (b) curves for Zn-H_2BDC/H_3BTC

Adsorption study

Effect of initial concentration: The adsorption performance of Zn-H_2BDC/H_3BTC toward cationic malachite green (MG) and anionic acid orange 7 (AO7) at different initial dye concentrations is shown in Fig. 4a. For both dyes, the adsorption capacity increased with increasing dye concentration, indicating enhanced mass transfer and greater interaction between dye molecules and the active adsorption sites of the MOF. The maximum adsorption capacities obtained at an initial concentration of 18 mg/L were 0.42 mg/g for MG and 1.90 mg/g for AO7. The consistently higher adsorption capacity observed for AO7 compared with MG across all investigated concentrations suggests a stronger affinity of Zn-H_2BDC/H_3BTC toward the anionic dye. This behaviour may be attributed to stronger electrostatic interactions and favourable surface interactions between AO7 molecules and the MOF framework.

Effect of pH: Th pH of the solution reportedly affects an adsorbents surface charges and influences the adsorbate/adsorbent interaction [23]. The effect of pH on the adsorption capacity of Zn-H_2BDC/H_3BTC for the adsorption of MG and AO7, studied in the pH range 3 to 10, is shown in Fig. 4b. The highest AO7 adsorption capacity value of 1.22 mg/g at pH 3 was achieved while the least AO7 adsorption capacity value of 1.06 mg/g at pH 10 was obtained. This implies that, at acidic pH, the extent of adsorption of anionic species, barring other factors that influences adsorption, has a direct correlation with the concentration of H^+ ions on adsorbent surface. Thus, the higher the concentration of hydrogen ion on the adsorbent surface, the higher the adsorption. Here, adsorption of AO7 is influenced by electrostatic interaction between hydrogen ions on the adsorbent surface and the anionic dye molecules [5]. At alkaline pH, where hydroxide ions cover adsorbent surfaces, adsorption of anionic species is inhibited by repulsion forces between hydroxide ions and the anionic species [5]. For MG, the highest adsorption capacity value, 0.65 mg/g, was obtained at alkaline pH 10 and the lowest value, 0.36 mg/g, at acidic pH 5. At alkaline pH, adsorption of cationic species is enhanced by electrostatic attraction forces between hydroxide ions and the cationic species. On the other hand, acidic pH does not favour the adsorption of cationic species as repulsion forces between positive H^+ ions and the cationic species inhibit adsorption [41]. The higher adsorption of AO7 relative to MG, observed across all pH studied, could be suggesting the influence of an accompanying factor, π-π interaction between the aromatic rings of Zn-H_2BDC/H_3BTC and those of the investigated dyes. A relatively poorer interaction between

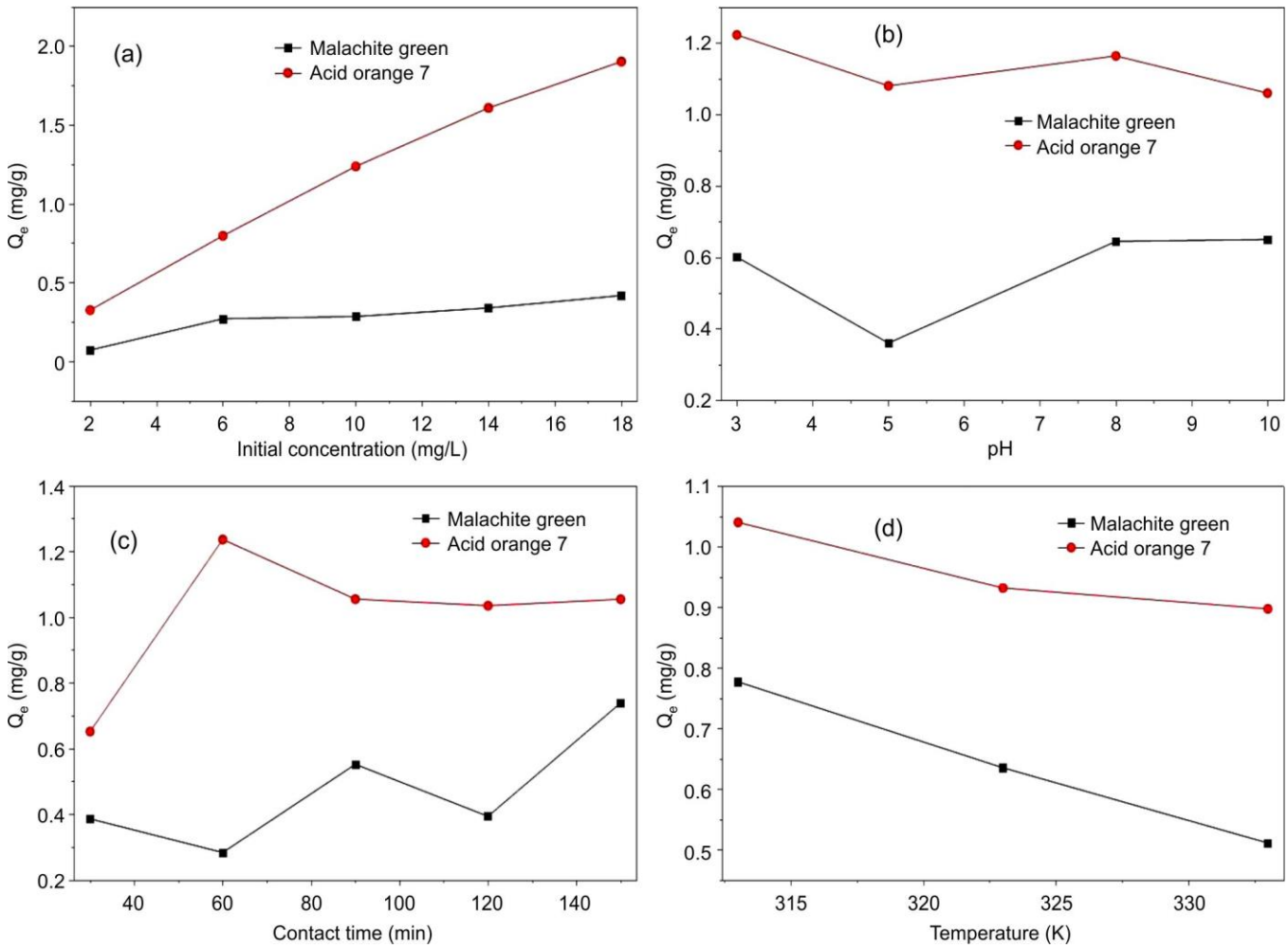

Fig. 4. Plots of adsorption capacity (Q_e) of Zn-H_2BDC/H_3BTC with (a) initial concentration (b) pH (c) contact time (d) temperature for malachite green and acid orange 7

aromatic rings of MG and those of Zn-H_2BDC/H_3BTC, due to steric hindrance of the amide functions, may have accounted for the lower adsorption of MG by Zn-H_2BDC/H_3BTC.

Effect of contact time: The effect of adsorbate/adsorbent contact time on the adsorption of AO7 and MG onto Zn-H_2BDC/H_3BTC was investigated at varying contact times between 30 to 120 min. The results (Fig. 4c) revealed that adsorption of AO7 attained maximum value at 60 min, with decreased adsorption observed at 90 min, which remained almost unchanged for the remaining contact times. In contrast, the adsorption of MG increased gradually with increasing contact time, exhibiting slight fluctuations before reaching its maximum adsorption capacity at 150 min. This reflects a slower adsorption of MG by Zn-H_2BDC/H_3BTC, relative to AO7.

Effect of temperature: The effect of temperature on the adsorption of MG and AO7 by Zn-H_2BDC/H_3BTC was studied at varying temperatures from 313 to 333 K. The results (Fig. 4d) shows that the adsorption of each dye onto Zn-H_2BDC /H_3BTC decreased as temperature increased, indicating a weakening of the attractive forces between dye and Zn-H_2BDC/ H_3BTC as temperature increased [42].

Equilibrium isotherms: The mathematical relationship between adsorption capacity (Q_e) and equilibrium concentration of dye solution (C_e) can be used to determine mathematical parameters, which are used to quantify the performances of adsorbents. These mathematical relationships are called adsorption or equilibrium isotherms [43]. A number of equilibrium isotherm models were utilised for the adsorption data:

Langmuir isotherm:

$$\frac{1}{Q_e} = \frac{1}{C_e Q_m K_L} + \frac{1}{Q_m} \quad (2)$$

Freundlich isotherm:

$$\ln Q_e = \ln K_F + \frac{1}{n} \ln C_e \quad (3)$$

Temkin isotherm:

$$Q_e = \frac{RT}{b} \ln C_e + \frac{RT}{b} \ln K_T \quad (4)$$

Elovich isotherm:

$$\ln \frac{Q_e}{C_e} = -\frac{Q_e}{Q_m} + \ln K_E Q_m \quad (5)$$

where Q_e and C_e represent the adsorption capacity and equilibrium concentration of the adsorbate, respectively. The isotherm constants obtained from the slope and intercept of the corresponding plots include Q_m (mg/g) and K_L (L/mg) for the Langmuir model, representing the maximum monolayer adsorption capacity and Langmuir constant, respectively [43,44]. In the Freundlich model, K_F (mg/g)(L/mg)$^{1/n}$ and n (dimensionless) denote the adsorption capacity and adsorption intensity, respectively [23,26,27]. For the Temkin model, b (J/mol) relates to the heat of adsorption, while K_T (L/g) is the Temkin equilibrium constant; R and T represent the gas constant and absolute temperature, respectively [27,45]. In the Elovich model, Qm (mg/g) and K_E (L/mg) correspond to the maximum adsorption capacity and Elovich constant, respectively [43,44].

The adsorption equilibrium studies were conducted to evaluate the extent and favourability of dye adsorption onto Zn-H_2BDC/H_3BTC. The equilibrium data were analysed using Langmuir, Freundlich, Temkin and Elovich isotherm models, as presented in Tables 1 and 2. Among them, the Langmuir isotherm model (Fig. 5) showed good agreement with the experimental data, with correlation coefficient (R^2) values of 0.9670 for MG and 0.9873 for AO7, indicating favourable monolayer adsorption on a homogeneous surface. The maximum adsorption capacity (Q_m) obtained for AO7 (1.848 mg/g) was higher than that of MG (1.469 mg/g), demonstrating the greater affinity of Zn-H_2BDC/H_3BTC toward AO7. The Langmuir constant (K_L) was further used to estimate the thermodynamic equilibrium constant (K_e^0) and Gibb's free energy change (ΔG^o) of the adsorption process using the following relations:

$$K_e^o = \frac{\text{Molecular weight of adsorbate} \times K_L \times c_o}{\gamma} \quad (15)$$

and

$$\Delta G^o = -RT \ln K_e^o \quad (16)$$

where K_e^0 is the equilibrium constant (a unitless quantity) the adsorbate; K_L is Langmuir isotherm constant in units of L/g

TABLE-1
LANGMUIR ISOTHERM PARAMETERS DERIVED FOR THE ADSORPTION OF MALACHITE GREEN AND ACID ORANGE 7 DYES ONTO Zn- H_2BDC/H_3BTC

	R^2	Q_m (mg/g)	K_L (L/mg)	R_L	K_e^0	ΔG^o (kJ)
Malachite green	0.9670	1.469	0.031	0.64	28,737.9	-25.43
Acid orange 7	0.9823	1.848	0.556	0.09	194,777.9	-30.18

TABLE-2
FREUNDLICH, TEMKIN AND ELOVICH ISOTHERMS PARAMETERS DERIVED FOR THE ADSORPTION OF MALACHITE GREEN

	Freundlich			Temkin			Elovich		
	R^2	K_F (mg/g) (L/mg)$^{1/n}$	n	R^2	K_T (L/g)	b (kJ/mol)	R^2	K_E (L/mg)	Q_m (mg/g)
Malachite green	0.8971	0.059	1.364	0.9444	1.111	17.969	0.3530	0.083	0.655
Acid orange 7	0.9978	0.560	1.733	0.9309	3.932	4.999	0.9104	0.729	1.269

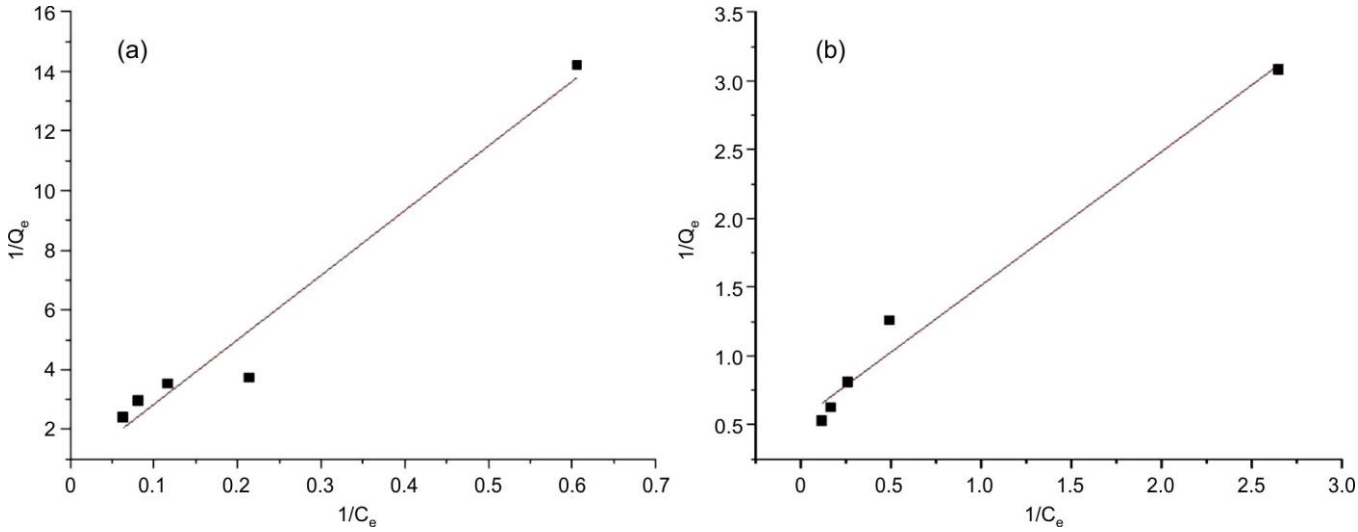

Fig. 5. Langmuir adsorption isotherm plots of malachite green (a) and acid orange 7 (b)

(obtained by multiplying K_L in units of L/mg by 1000); c_o is the molar concentration of the adsorbate solution (1 mol/L), γ is also a unitless quantity equivalent to the activity coefficient. In dilute solutions, γ is assumed to be unity (*i.e.* $\gamma = 1$), R is the universal gas constant (8.314 J/K/mol) and T is the absolute temperature of the dye solutions studied (at 298 K) [46,47].

The parameter, R_L is a dimensionless factor, known as the separation factor and is useful for evaluating the favourability of an adsorption system [43]. And R_L is related to K_L by the relation:

$$R_L = \frac{1}{1 + K_L C_o} \quad (17)$$

where C_o is initial concentration of adsorbent. The value of R_L indicates that the adsorption is unfavourable if $R_L > 1$, linear if $R_L = 1$, favourable if $0 < R_L < 1$ or irreversible if $R_L = 0$ [26,28].

The negative values of ΔG^o, -25.43kJ and -30.18kJ for MG and AO7, respectively, indicated that the adsorption were spontaneous. R_L values for the adsorption of both dyes, 0.64 and 0.09 for MG and AO7, respectively, lie between 0 and 1, indicating favourability of their respective adsorption.

The Freundlich isotherm (Fig. 6) also showed good agreement with the adsorption data, with R^2 values of 0.8971 for MG and 0.9978 for AO7, indicating favourable heterogeneous adsorption. The applicability of both Langmuir and Freundlich models suggests the coexistence of monolayer and multilayer adsorption mechanisms during dye uptake [48]. The Freundlich adsorption constant (K_F) was higher for AO7 (0.56) than for MG (0.059), confirming the greater adsorption affinity of Zn-H_2BDC/H_3BTC toward AO7. The adsorption intensity parameter (n) was 1.364 for MG and 1.733 for AO7, indicating moderately favourable adsorption for both dyes [49].

The Temkin isotherm (Fig. 7) was used to evaluate the heat of adsorption, assuming that the adsorption energy decreases linearly with surface coverage [45]. The positive b values obtained for MG (17.969 kJ/mol) and AO7 (4.999 kJ/mol) indicate that the adsorption processes were exothermic in nature.

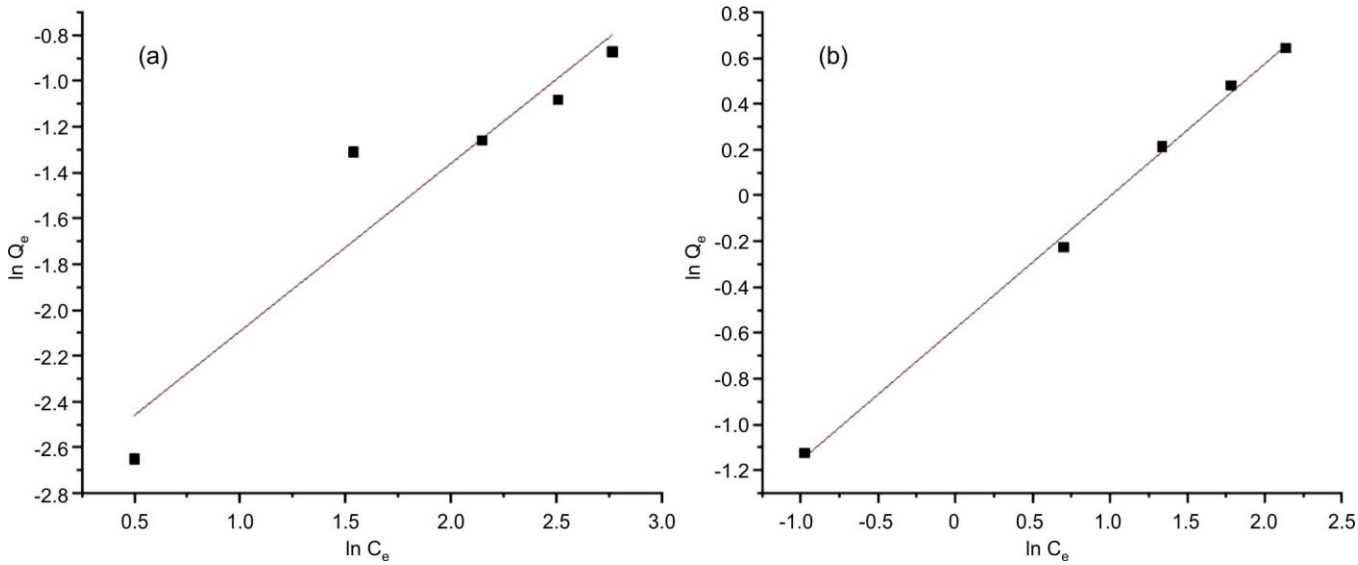

Fig. 6. Freundlich adsorption isotherm plots of malachite malachite green (a) and acid orange 7 (b)

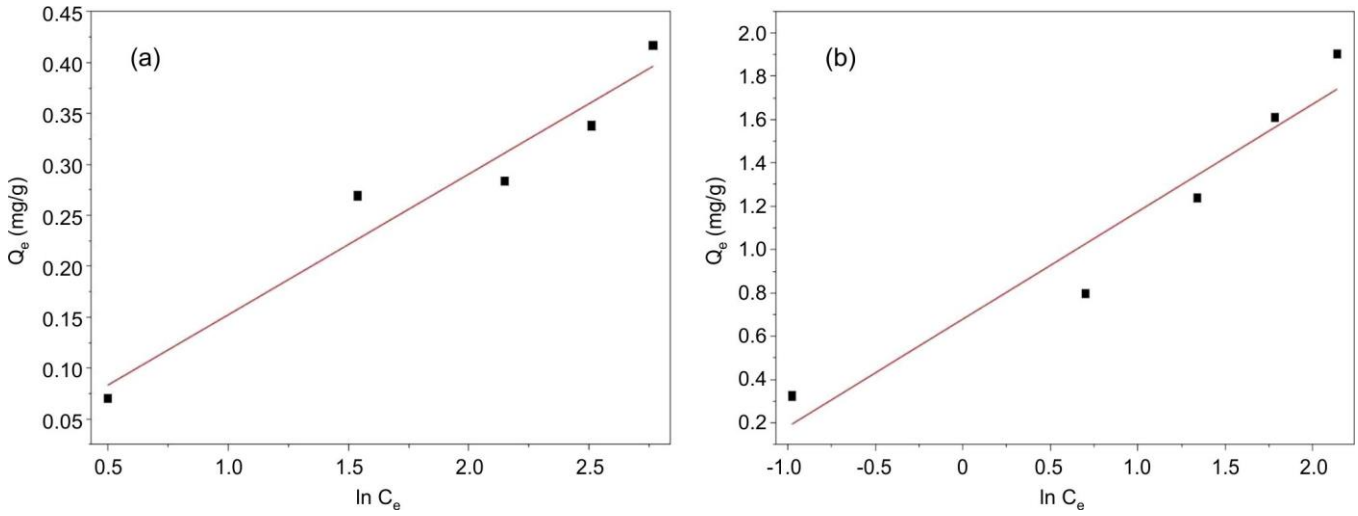

Fig. 7. Temkin adsorption isotherm plots of malachite green (a) and acid orange 7 (b)

The higher Temkin constant (K_T) observed for AO7 (3.932 L/g) compared with MG (1.111 L/g) suggests stronger adsorbate–adsorbent interactions and preferential binding of AO7 onto the active sites of the MOF [50,51].

The Elovich isotherm (Fig. 8), which describes multilayer adsorption on heterogeneous surfaces [43], further supported the adsorption behaviour of the investigated dyes. The calculated Elovich maximum adsorption capacities (Q_m) were 0.655 mg/g for MG and 1.269 mg/g for AO7, again demonstrating the higher adsorption affinity toward AO7. The Elovich constant (K_E), related to the initial adsorption rate, was also higher for AO7 (0.729 L/mg) than for MG (0.083 L/mg), indicating faster uptake of AO7 molecules by the adsorbent.

Comparative studies: Comparison of the adsorption capacities of Zn-H_2BDC/ H_3BTC Zn-H_2BDC/H_3BTC with previously reported MOFs of similar ligand composition (Table-3) revealed comparatively lower adsorption performance toward both dyes. Although the synthesized MOF exhibited relatively small crystallite size (22.69 nm) and expected high surface area characteristics, the adsorption effici-

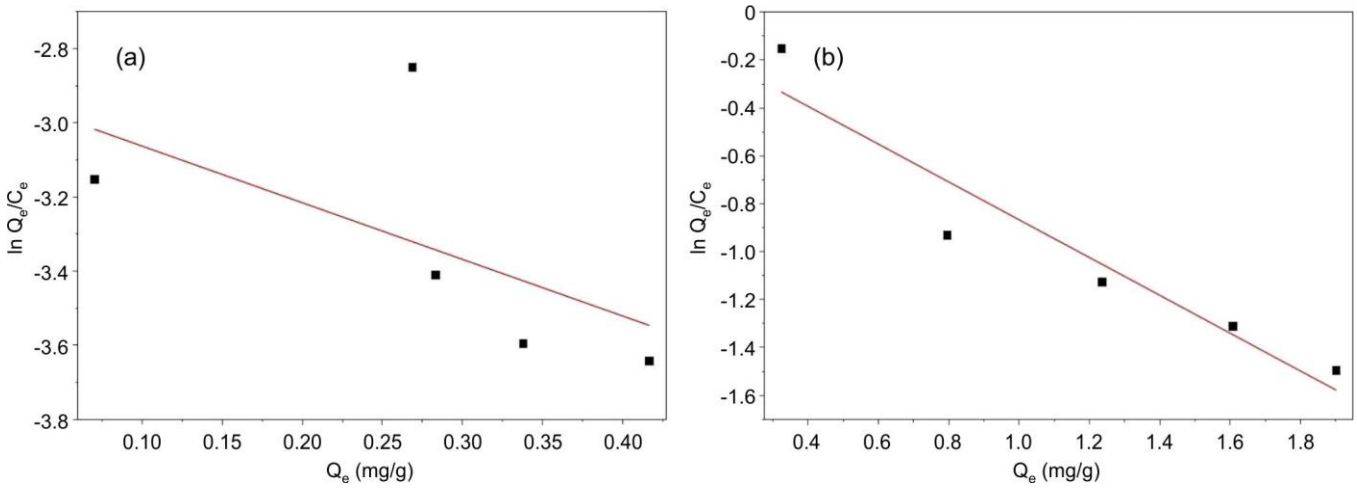

Fig. 8. Elovich adsorption isotherm plots of malachite green (a) and acid orange 7 (b)

TABLE-3
COMPARISON OF MALACHITE GREEN AND ACID ORANGE 7 ADSORPTION PERFORMANCES OF MOFs SIMILAR TO Zn-H_2BDC/H_3BTC IN LIGAND COMPOSITION

MOF	Dyes	Q_m (mg/g)	Equilibration time (min)	Ref.
Zn-H_2BDC/H_3BTC	Malachite green	1.848	60	Current study
	Acid orange 7	1.469	60	Current study
Fe-BTC	Malachite green	177	30	[45]
	Malachite green	205	120	[55]
Fe-BTC	Acid orange 7	409.84	4,320	[56]
Cu-BTC	Malachite green	4.7	10	[57]
Cu-BTC/BDC	Malachite green	185	60	[26]
Zr-BDC	Acid orange 7	106.6	1440	[58]

ency remained limited. This suggests that adsorption performance is influenced not only by crystallite size and porosity but also by factors such as pore accessibility, surface properties and effective exposure of adsorption sites [26,52,53]. The relatively poor adsorption performance of Zn-H_2BDC/H_3BTC may therefore be associated with particle compaction or restricted accessibility of active sites to dye molecules [54]. Nevertheless, the present study successfully demonstrated the comparatively stronger adsorption affinity of the synthesized MOF toward the anionic dye AO7 relative to the cationic dye MG.

Adsorption kinetics: The effect of contact time on the adsorption process was investigated using various kinetic models to understand the adsorption mechanism and evaluate parameters such as adsorption capacity and adsorption rate. The adsorption kinetic models are generally classified into reaction-based and diffusion-based models, depending on the controlling mechanism governing the adsorption process [59]. The linear equations of both kinds of models employed in this study are:

Pseudo-first order (PFO) kinetics:

$$\ln (Q_e - Q_t) = \ln Q_e - K_1 t \quad (7)$$

Pseudo-second order (PSO) kinetics:

$$\frac{t}{Q_t} = \frac{1}{K_2 Q_e^2} + \frac{t}{Q_e} \quad (8)$$

Weber-Morris intraparticle diffusion:

$$Q_t = K_{id}\sqrt{t} + c \quad (9)$$

where Q_e (mg/g) is the weight of dye adsorbed per gram of Zn-H_2BDC/H_3-BTC at equilibrium; Q_t (mg/g) is the weight of dye adsorbed per gram of Zn-H_2BDC/H_3-BTC at time, t; K_1 (min^{-1}), K_2 (mg/g/min) and K_{id} are the rate constant of the pseudo-first order, pseudo-second order and the intraparticle diffusion models, $\sqrt{t}$ is the square root of the contact time and C is the thickness of the boundary layer [59-61].

The linear plots of the pseudo-first order (PFO), pseudo-second order (PSO) and intraparticle diffusion are shown in Figs. 9-11. The values of their respective parameters obtained from their respective plots are presented in Table-4. In the PFO kinetic modelling of adsorption of MG and AO7 (Fig. 9), the coefficient of determination, R^2, values were 0.2215 and 0.0120 for MG and AO7, respectively. These values depict a poor fitting and inadequacy of the model to describe the kinetics of adsorption of both dyes.

In the PSO kinetic modelling (Fig. 10), R^2 values were 0.4346 and 0.9578, for MG and AO7, respectively. These values, in comparison to those from the PFO signifies a better fit to the kinetic data. A value of 0.9578 for AO7 shows PSO was the rate limiting step in the adsorption of AO7 onto Zn-H_2BDC/H_3BTC. As a further confirmation, the Q_e value, 1.154 mg/g, quite agrees with the experimental value of 1.057 mg/g. In terms of the PSO rate constants, K_2, the value for AO7 (0.078) is greater than the value for MG (0.015), thus, indicating a faster adsorption of AO7 relative to MG. The moderate R^2 value of 0.4346 for MG indicate that, to some extent, PSO kinetics occurred, although, not the rate limiting step. The intraparticle diffusion (IPD) modelling of both dyes (Fig. 11)

TABLE-4
PFO, PSO AND IPD PARAMETERS DERIVED FROM THE ADSORPTION OF MALACHITE GREEN AND ACID ORANGE 7 ONTO Zn-H_2BDC/H_3BTC

	Pseudo first order			Pseudo second order			Intra-particle diffusion		
	R^2	Q_e (mg/g)	K_1 (g/mg/min)	R^2	Q_e (mg/g)	K_2 (g/mg/min)	R^2	C (mg/g)	K_2 (g/mg/min)
Malachite green	0.2215	0.234	-0.006	0.4346	0.873	0.015	0.4643	0.053	0.046
Acid orange 7	0.0120	7.674	0.013	0.9578	1.154	0.078	0.2734	0.620	0.042

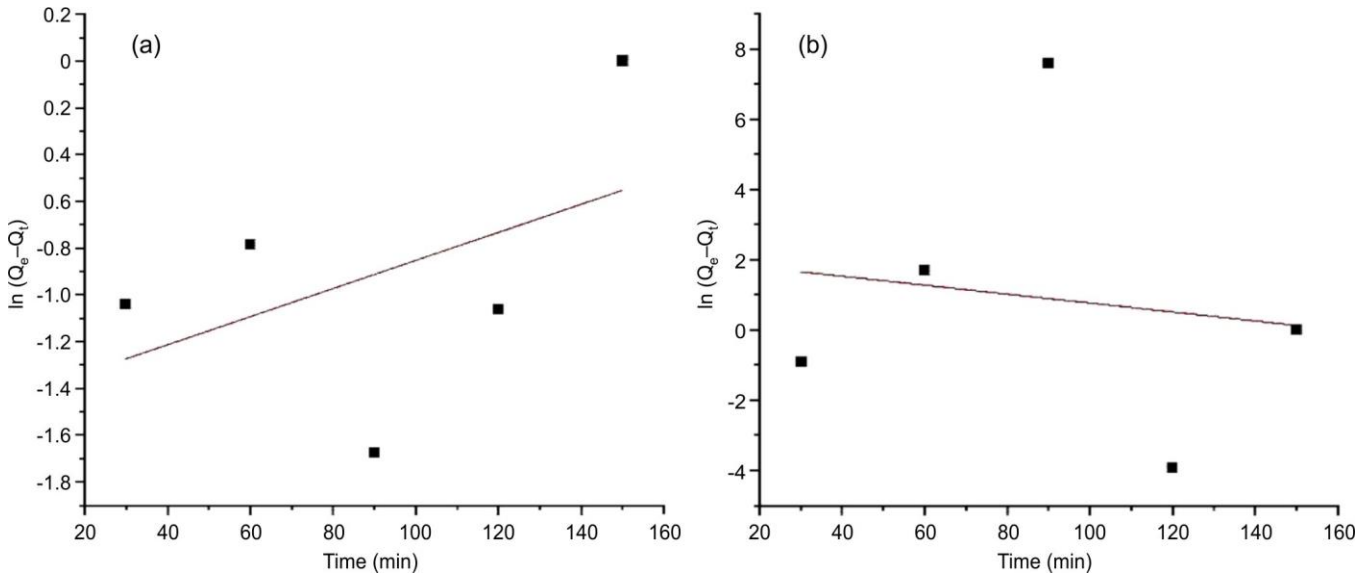

Fig. 9. Pseudo first order kinetic plots for adsorption of malachite green (a) and acid orange 7 (b) onto Zn-H_2BDC/H_3BTC

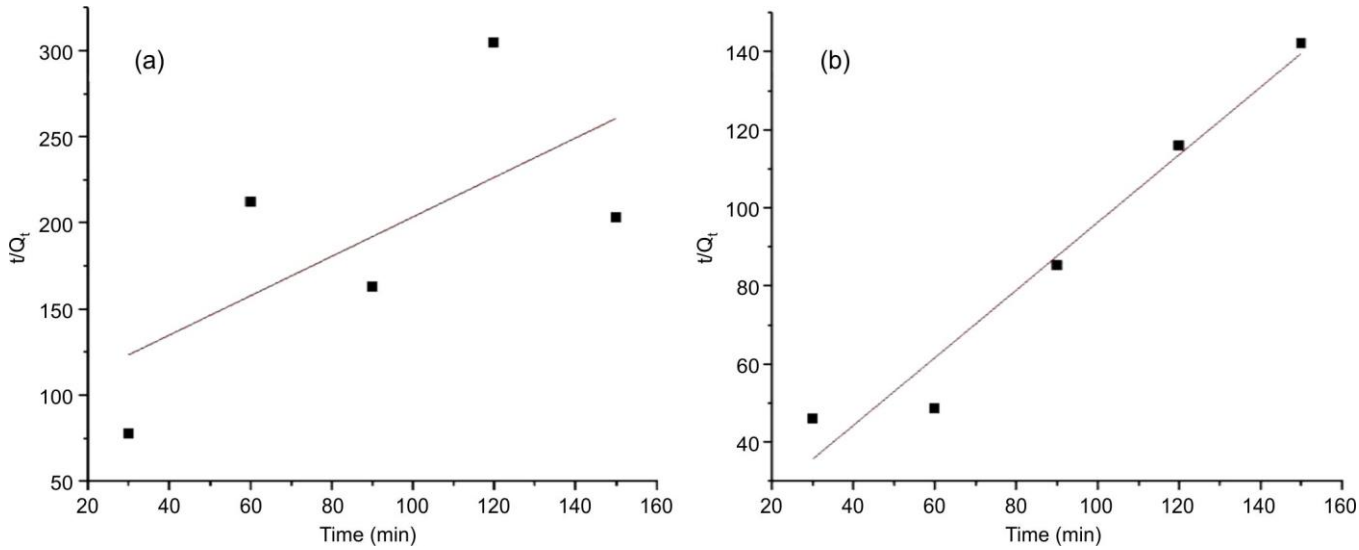

Fig. 10. Pseudo second order kinetic plots for adsorption of malachite green (a) and acid orange 7 (b) onto Zn-H_2BDC/H_3BTC

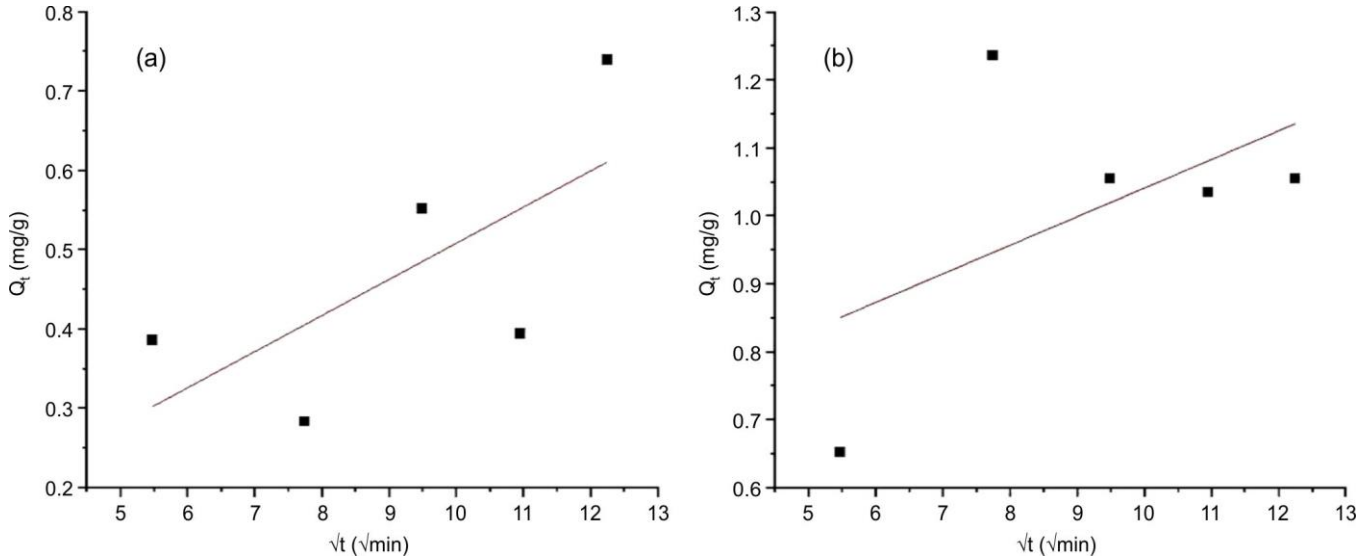

Fig. 11. Intraparticle diffusion plots for adsorption of malachite green (a) and acid orange 7 (b) onto Zn-H_2BDC/H_3BTC

yielded R^2 values of 0.4643 and 0.2734 for MG and AO7, respectively. The higher R^2 value from the IPD modelling obtained for MG compared to those from the kinetic models (PFO and PSO) indicates that IPD was the rate limiting step. Further, the IPD constant, C, is closer to zero (C=0.053). This signals that IPD was the rate limiting step in the adsorption of MG. For AO7, the lower R^2 value compared to that from the PSO, indicates that IPD was not the rate limiting step in its adsorption. The C value of 0.620, show that the best fit line is quite away from the origin, as a further proof that intraparticle diffusion was not the rate limiting step. With the kinetic figures favouring PSO, it is quite evident that the rate limiting step was PSO and controlled by chemisorptive interactions [16,22] between the dye and Zn-H_2BDC/H_3BTC.

Adsorption thermodynamics: The experimental data obtained from the study on the effect of temperature on adsorption are useful for determining thermodynamic parameters used in the description of adsorption processes from a thermodynamic perspective. Thermodynamic of adsorption is concerned mostly with the determination of the heat of adsorption and prediction of the spontaneity and/or feasibility of an adsorption process. The following parameters: isosteric heat of adsorption (ΔH_x), activation energy (E_a), sticking probability (S^*) and change in standard Gibb's free energy (ΔG^o), change in enthalpy (ΔH^o) and change in entropy (ΔS^o) were determined from the following linear equations:

Clausius-Clapeyron equation:

$$\ln C_e = -\left[\frac{\Delta H_x}{R}\right]\frac{1}{T} + K \quad (10)$$

Arrhenius equation:

$$\ln(1-\theta) = \ln S^* + \left[\frac{E_a}{R}\right]\frac{1}{T} \quad (11)$$

Van't Hoff equation:

$$\ln K_c = \frac{\Delta S^o}{R} - \left[\frac{\Delta H^o}{R}\right]\frac{1}{T} \quad (12)$$

Josiah Willard Gibbs equation:

$$\Delta G^o = \Delta H^o - T\Delta S^o \quad (13)$$

where K is a constant; R (joule) is gas constant; C_e (mg/L) is equilibrium concentration; T (K) is absolute temperature; and ΔH_x is the isosteric heat of adsorption calculated from the slope of the plot of ln C_e *versus* 1/T (eqn. 10); θ (eqn. 11) is the surface coverage ($\theta = 1 - C_e/C_o$ where C_e and C_o are equilibrium and initial concentrations, respectively); E_a and S^*, derived from the slope and intercept of the Arrhenius equation (eqn. 12), are the activation energy and sticking probability; ΔG^o, ΔH^o and ΔS^o, derived from the Gibb's equation (eqn. 13), are the change in standard Gibb's free energy, change in enthalpy and change in entropy, respectively.

The thermodynamic parameters derived from the experimental adsorption data are presented in Tables 5 and 6, while the corresponding thermodynamic plots are shown in Figs. 12-14. The evaluated parameters included the standard Gibbs free energy change (ΔG^o), enthalpy change (ΔH^o), entropy change (ΔS^o), isosteric heat of adsorption (ΔH_x), activation energy (E_a) and sticking probability (S^*). These parameters provide important information regarding the spontaneity, adsorption mechanism and adsorbate-adsorbent interactions [59].

The negative values of ΔG^o and ΔH^o obtained for both MG and AO7 adsorption indicate that the adsorption processes were spontaneous and exothermic in nature. AO7 exhibited more negative ΔG^o values than MG, suggesting a comparatively higher degree of spontaneity and stronger affinity toward Zn-H_2BDC/H_3BTC. The magnitude of ΔG^o values (-11.07 to -14.15 kJ/mol) further suggests that adsorption predominantly occurred through physisorption mechanisms [42]. The positive ΔS^o values indicate increased randomness at the solid-solution interface during adsorption. The isosteric heat of adsorption (ΔG_x) values for MG and AO7 were 8.55 and 6.05 kJ/mol, respectively, which are significantly lower than 80 kJ/mol, confirming weak adsorbate-adsorbent interactions characteristic of physisorption. Similarly, the low negative activation energy (E_a) values indicate a low energy barrier for adsorption, suggesting that dye molecules can be readily adsorbed onto the MOF surface. The higher magnitude of E_a for MG indicates a slightly greater adsorption tendency compared with AO7.

TABLE-5
VALUES OF PARAMETERS FROM VAN'T HOFF EQUATION, ΔH, ΔS AND ΔG FOR MALACHITE GREEN AND ACID ORANGE 7 ADSORPTIONS ONTO Zn-H_2BDC/H_3BTC

Dye	ΔH (kJ/mol)	ΔS (kJ/k/mol)	ΔG (kJ/mol)			R^2
			313 K	323 K	333 K	
Malachite green	-26.72	-0.05	-11.07	-10.57	-10.07	0.9999
Acid orange 7	-12.48	0.005	-14.05	-14.10	-14.15	0.9279

TABLE-6
VALUES OF PARAMETERS FROM CLAUSIUS-CLAPEYRON AND ARRHENIUS EQUATIONS, ΔH_x, E_a AND S*, FOR MALACHITE GREEN AND ACID ORANGE 7 ADSORPTIONS ONTO Zn-H_2BDC/H_3BTC

	Clausius-Clapeyron equation parameters			Arrhenius equation parameters		
	ΔH_x (kJ/mol)	K	R^2	S*	E_a (kJ/mol)	R^2
Malachite green	8.55	5.10	0.9977	16.365	-8.55	0.9977
Acid orange 7	6.05	3.90	0.9204	4.956	-6.05	0.9204

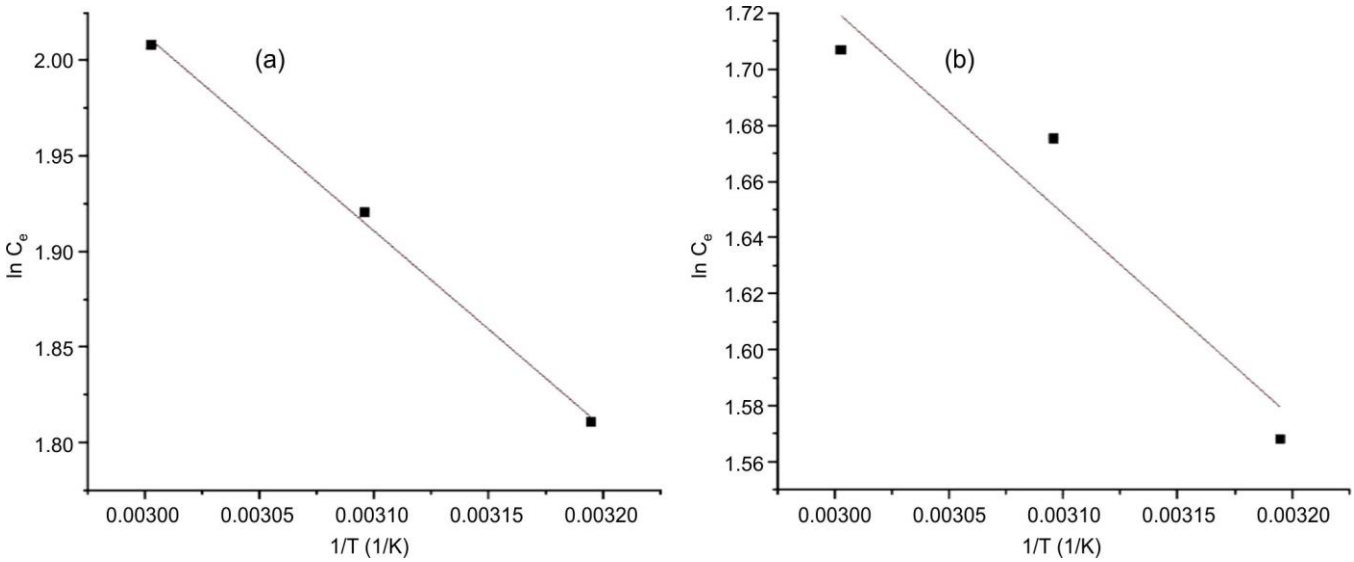

Fig. 12. Clausius-Clapeyron equation plots (ln C_e *vs.* 1/T) for the determination of isosteric heat of adsorption of malachite green (a) and acid orange 7 (b)

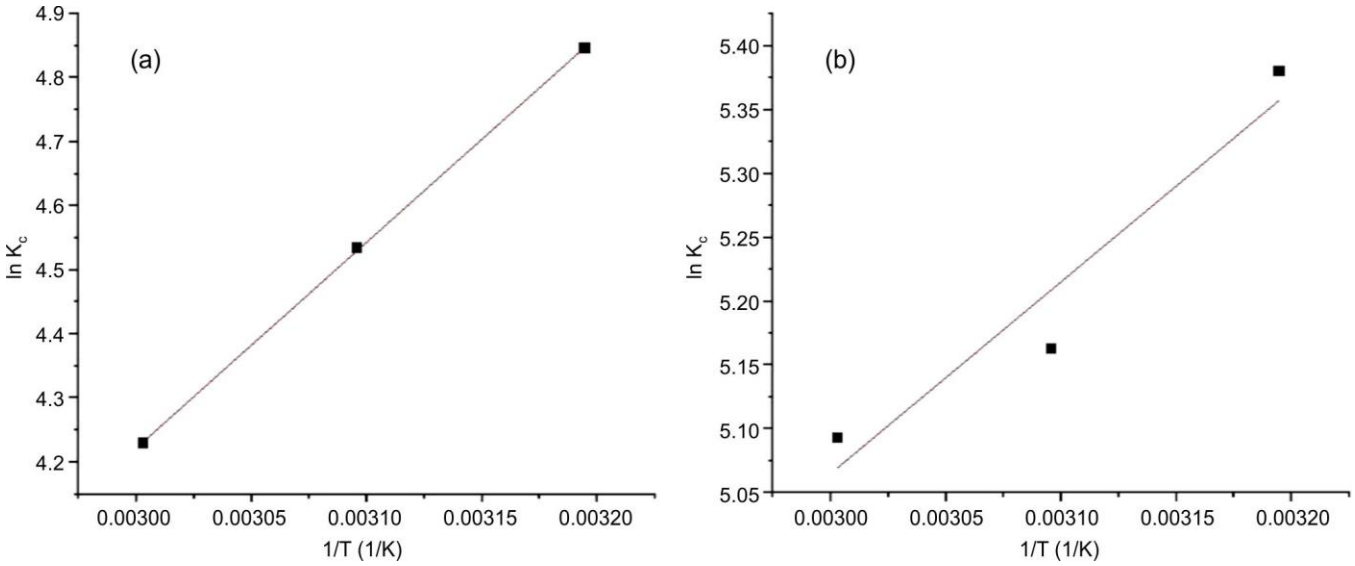

Fig. 13. van't Hoff equation plots (ln K_c *vs.* 1/T) for the determination of ΔH^o and ΔS^o in the adsorption of malachite green (a) and acid orange 7 (b)

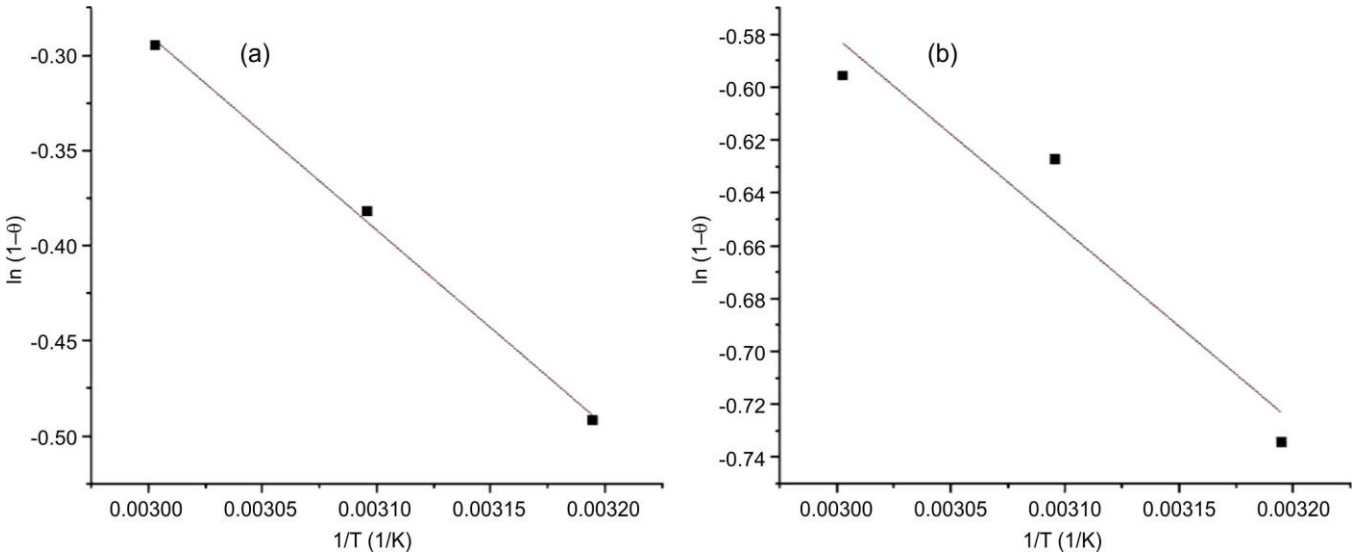

Fig. 14. Arrhenius equation plots (ln (1–θ) *vs.* 1/T) for the determination of sticking probability and activation energy of adsorption of malachite green (a) and acid orange 7 (b)

The sticking probability (S^*) values obtained for MG (16.365) and AO7 (4.956) were higher than unity, indicating weak sticking tendency and relatively low interaction strength between the dye molecules and Zn-H_2BDC/H_3BTC. These findings collectively confirm that the adsorption process is spontaneous, exothermic and mainly governed by weak physical interactions.

Conclusions

This study successfully synthesized the metal-organic framework Zn-H_2BDC/H_3BTC *via* a solvothermal approach and evaluated its adsorption behaviour toward cationic malachite green (MG) and anionic acid orange 7 (AO7) dyes. FTIR analysis confirmed the successful coordination between Zn ions and the organic linkers, while PXRD and TGA/DTG analyses demonstrated the crystalline nature and adequate thermal stability of the synthesized framework. Adsorption studies revealed that dye uptake increased with increasing initial dye concentration. The adsorption of AO7 was favoured under acidic conditions, whereas MG adsorption increased under alkaline conditions. Under all investigated experimental conditions, Zn-H_2BDC/H_3BTC exhibited greater adsorption affinity toward AO7 than MG. Equilibrium was attained within 60 min for AO7 adsorption, while MG adsorption gradually increased up to 150 min. The adsorption equilibrium data were satisfactorily described by both Langmuir and Freundlich isotherm models, indicating the coexistence of monolayer and heterogeneous multilayer adsorption processes. The higher Langmuir adsorption capacity obtained for AO7 confirmed the preferential adsorption of the anionic dye. Temkin and Elovich models further supported the exothermic nature of adsorption and the comparatively faster uptake of AO7 molecules. Kinetic analysis indicated that intraparticle diffusion significantly influenced MG adsorption, whereas pseudo-second-order kinetics

predominated during AO7 adsorption. Thermodynamic studies demonstrated that the adsorption processes were spontaneous, exothermic and mainly governed by weak physisorption interactions. The relatively higher adsorption affinity of Zn-H_2BDC/H_3BTC toward AO7 suggests its potential applicability as a selective adsorbent for anionic dye removal from aqueous systems.

ACKNOWLEDGEMENTS

The authors express their appreciations to the following individuals: Prof. F. Sikoki, Dean Faculty of Basic and Applied Science, University of Africa, Toru-Orua, Bayelsa State, Nigeria; Prof. T.J.F. Tarawo, Dean, Faculty of Science, Niger Delta University, Bayelsa State, Nigeria; and Mr Daniel Ziriki, Chief Laboratory Technologist, Chemistry Laboratory, University of Africa, Toru-Orua, Bayelsa State, Nigeria.

CONFLICT OF INTEREST

The authors declare that there is no conflict of interests regarding the publication of this article.

DECLARATION OF AI-ASSISTED TECHNOLOGIES

During the preparation of this manuscript, the authors used an AI-assisted tool(s) to improve the language. The authors reviewed and edited the content and take full responsibility for the published work.

REFERENCES

1. E.B. AttahDaniel, F.M. Mtunzi, D. Wankasi, N. Ayawei, E.D. Dikio and P.N. Diagboya, *Water Air Soil Pollut.*, **233**, 442 (2022); https://doi.org/10.1007/s11270-022-05912-2
2. G.D.A. Umbuzeiro, A.E. Albuquerque, F.I. Vacchi, M. Szymczyk, X. Sui, R. Aalizadeh, P.C. von der Ohe, N.S. Thomaidis, N.R. Vinueza and H.S. Freeman, *Environ. Sci. Eur.*, **31**, 76 (2019); https://doi.org/10.1186/s12302-019-0258-1
3. M.W. Ashraf, N. Abulibdeh and A. Salam, *Int. J. Environ. Res. Public Health*, **16**, 3484 (2019); https://doi.org/10.3390/ijerph16183484
4. M. Berradi, R. Hsissou, M. Khudhair, M. Assouag, O. Cherkaoui, A. El Bachiri and A. El Harfi, *Heliyon*, **5**, e02711 (2019); https://doi.org/10.1016/j.heliyon.2019.e02711
5. S.J. Salih, A.S. Abdul Kareem and S.S. Anwer, *Heliyon*, **8**, e10092 (2022); https://doi.org/10.1016/j.heliyon.2022.e10092
6. B. Lellis, C.Z. Fávaro-Polonio, J.A. Pamphile and J.C. Polonio, *Biotechnol. Res. Innov.*, **3**, 275 (2019); https://doi.org/10.1016/j.biori.2019.09.001
7. N.P. Raval, P.U. Shah and N.K. Shah, *Appl. Water Sci.*, **7**, 3407 (2017); https://doi.org/10.1007/s13201-016-0512-2
8. D.A. Yaseen and M. Scholz, *Environ. Sci. Pollut. Res. Int.*, **25**, 1980 (2018); https://doi.org/10.1007/s11356-017-0633-7
9. A.A. Adeyi, S.N.A.M. Jamil, L.C. Abdullah and T.S.Y. Choong, *J. Chem.*, **2019**, 4321475 (2019); https://doi.org/10.1155/2019/4321475
10. X. Zhang, Z. Chen, X. Liu, L. Silvia, X. Wang, R. Taheri-Ledari, A. Maleki, P. Li and O.K. Farha, *Chem. Soc. Rev.*, **49**, 7406 (2020); https://doi.org/10.1039/D0CS00997K
11. O.M. Yaghi, M.J. Kalmutzki and C.S. Diercks, Introduction to Reticular Chemistry: Metal-Organic Frameworks and Covalent Organic Frameworks, Wiley-VCH Verlag GmbH& Co., edn 1 (2019). https://doi.org/10.1002/9783527821099
12. G. Férey, *Chem. Soc. Rev.*, **37**, 191 (2008); https://doi.org/10.1039/B618320B
13. V.K.M. Au, *Front Chem.*, **8**, 708 (2020); https://doi.org/10.3389/fchem.2020.00708
14. J.L.C. Rowsell, E.C. Spencer, J. Eckert, J.A.K. Howard and O.M. Yaghi, *Science*, **309**, 5739 (2005); https://doi.org/10.1126/science.1113247
15. S. Ukachuku and D.E. Dikio, *World News Nat. Sci.*, **49**, 2023 (2023); https://doi.org/10.1007/s15033-023-3526-0
16. C. Wang, X. Liu, T. Yang, D. Sridhar, H. Algadi, B.X. Bin, Z.M. El-Bahy, H. Li, Y. Ma, T. Li and Z. Guo, *Sep. Purif. Technol.*, **320**, 124144 (2023); https://doi.org/10.1016/j.seppur.2023.124144
17. S. Rojas and P. Horcajada, *Chem. Rev.*, **120**, 8378 (2020); https://doi.org/10.1021/acs.chemrev.9b00797
18. F.C. Tsai, Y. Xia, N. Ma, J.J. Shi, T. Jiang, T.C. Chiang, Z.C. Zhang and W.C. Tsen, *Desalin. Water Treat.*, **57**, 3218 (2016); https://doi.org/10.1080/19443994.2014.982199
19. S. He, L. Wu, X. Li, H. Sun, T. Xiong, J. Liu, C. Huang, H. Xu, H. Sun, W. Chen, R. Gref and J. Zhang, *Acta Pharm. Sin. B*, **11**, 2362 (2021); https://doi.org/10.1016/j.apsb.2021.03.019
20. I. Kritskiy, T. Volkova, A. Surov and I. Terekhova, *Carbohydr. Polym.*, **216**, 224 (2019); https://doi.org/10.1016/j.carbpol.2019.04.037
21. S. Loera-Serna and E. Ortiz, Catalytic Applications of Metal-Organic Frameworks, IntechOpen (2016);
22. S. Ukachuku, D.E. Amaebi and C.I. Dike, *J. Appl. Sci. Environ. Manag.*, **27**, 283 (2023); https://doi.org/10.4314/jasem.v27i2.14
23. A.S. Elsherbiny, A. Rady, R.M. Abdelhameed and A.H. Gemeay, *Environ. Sci. Pollut. Res.*, **30**, 106860 (2023); https://doi.org/10.1007/s11356-023-25919-4
24. S. Ukachuku and E.D. Dikio, *World Sci. News*, **181**, 99 (2023).
25. F.H. Wei, D. Chen, Z. Liang, S. Zhao and Y. Luo, *RSC Adv.*, **7**, 46520 (2017); https://doi.org/10.1039/C7RA09243A
26. Z. Shi, L. Li, Y. Xiao, Y. Wang, K. Sun, H. Wang and L. Liu, *RSC Adv.*, **7**, 30904 (2017); https://doi.org/10.1039/C7RA04820C
27. M. Puerto-Rodríguez, C. López-Cartes and R. Ayala, *J. Solid State Chem.*, **312**, 123260 (2022); https://doi.org/10.1016/j.jssc.2022.123260
28. K. Roztocki, I. Senkovska, S. Kaskel and D. Matoga, *Eur. J. Inorg. Chem.*, **2016**, 4450 (2016); https://doi.org/10.1002/ejic.201600134
29. C.K. Chang, T.R. Ko, T.Y. Lin, Y.-C. Lin and H.J. Yu, *Commun. Chem.*, **6**, 118 (2023); https://doi.org/10.1038/s42004-023-00917-2
30. J.S. Qin, S. Yuan, Q. Wang, A. Alsalme and H.C. Zhou, *J. Mater. Chem. A Mater. Energy Sustain.*, **5**, 4280 (2017); https://doi.org/10.1039/C6TA10281F
31. H. Chevreau, T. Devic, F. Salles, G. Maurin, N. Stock and C. Serre, *Angew. Chem. Int. Ed.*, **52**, 5056 (2013); https://doi.org/10.1002/anie.201300057
32. E.D. Dikio and A.M. Farah, *Chem. Sci. Trans.*, **2**, 1386 (2013).
33. F.T. Alshorifi, A.I. Ahmad and S.M. El Dafrawy, *Int. J. Nano Mater. Sci.*, **6**, 25 (2017).
34. T. Dutta, K.H. Kim, R.J.C. Brown, Y.H. Kim and D. Boukhvalov, *Sci. Rep.*, **8**, 3343 (2018); https://doi.org/10.1038/s41598-018-23391-6
35. I. Aamer, N. Iqbal, T. Noor and A. Asghar, *Mater. Res. Express*, **8**, 075601 (2021); https://doi.org/10.1088/2053-1591/ac14ff
36. F.T. Alshorifi, S.M. El Dafrawy and A.I. Ahmed, *ACS Omega*, **7**, 23421 (2022); https://doi.org/10.1021/acsomega.2c01770
37. T. Chen, A. Yang, W. Zhang, J. Nie, T. Wang, J. Gong, W. Wang and Y. Ji, *Nanomaterials*, **12**, 3234 (2022); https://doi.org/10.3390/nano12183234
38. M.Y. Kalashgrani, A. Babapoor, S.M. Mousavi, S. Feizpoor, S.A. Hashemi, M. Binazadeh, W.-H. Chiang and C.W. Lai, *Separations*, **10**, 261 (2023); https://doi.org/10.3390/separations10040261

39. A. Chinthamreddy, S. Koppula, S.B Nallamalla, G. Karra and S.B.M. Surya, *Chem. Phys. Impact*, **8**, 100599 (2024); https://doi.org/10.1016/j.chphi.2024.100599
40. Z. Anfar, M. Zbair, H.A. Ahsaine, Y. Abdellaoui, A.A. El Fakir, E.H. Amaterz, A. Jada and N. El Alem, *ChemistrySelect*, **4**, 4981 (2019); https://doi.org/10.1002/slct.201901043
41. N. Tripathi, *IOSR J. Appl. Chem.*, **5**, 91 (2013); https://doi.org/10.9790/5736-5391108
42. M. Horsfall Jnr. and A.I. Spiff, *Electron. J. Biotechnol.*, **8**, 162 (2005); https://doi.org/10.2225/vol8-issue2-fulltext-4
43. A. Abin-Bazaine, A.C. Trujillo and M. Olmos-Marquez, in eds.: M. Ince and O.K. Ince, Adsorption Isotherms: Enlightenment of the Phenomenon of Adsorption, IntechOpen (2022).
44. N. Ayawei, A.N. Ebelegi and D. Wankasi, *J. Chem.*, **2017**, 3039817 (2017); https://doi.org/10.1155/2017/3039817
45. S. Ukachuku and C.Y. Abasi, *Ann. Appl. Sci.*, **7**, 23 (2021).
46. E.C. Lima, A. Hosseini-Bandegharaei, J.C. Moreno-Piraján and I. Anastopoulos, *J. Mol. Liq.*, **273**, 425 (2019); https://doi.org/10.1016/j.molliq.2018.10.048
47. G.R. Delpiano, D. Tocco, L. Medda, E. Magner and A. Salis, *Int. J. Mol. Sci.*, **22**, 788 (2021); https://doi.org/10.3390/ijms22020788
48. B.A. Fil and S. Günaslan, *Bull. Chem. Soc. Ethiop.*, **37**, 223 (2022); https://doi.org/10.4314/bcse.v36i1.18
49. E. García, R. Medina, M. Lozano, P.I. Hernández, M. Valero and A. Franco, *Materials*, **7**, 8037 (2014); https://doi.org/10.3390/ma7128037
50. X. Zhou, R. Maimaitiniyazi and Y. Wang, *Arab. J. Chem.*, **15**, 104267 (2022); https://doi.org/10.1016/j.arabjc.2022.104267
51. M.S. Mohy Eldin, K.M. Aly, Z.A. Khan, A.E.M. Mekky and T.S. Saleh, Desalination *Water Treat.*, **57**, 56 (2016); https://doi.org/10.1080/19443994.2016.1171168
52. J. Yang, X. Tang J. Liu, J. Wang, H. Shang, L. Wu and J. Li, *Chem. Eng. J.*, **406**, 126599 (2021); https://doi.org/10.1016/j.cej.2020.126599
53. W. Jiang and K. Takeda, *Phys. Chem. Chem. Phys.*, **24**, 35 (2022); https://doi.org/10.1039/D1CP03922A
54. Y. Liu, J. Miao, H. Han and P. Xu, *ACS Omega*, **6**, 5886 (2021); https://doi.org/10.1021/acsomega.0c06306
55. F. Tan, M. Liu, K. Li, Y. Wang, J. Wang, X. Guo, G. Zhang and C. Song, *Chem. Eng. J.*, **281**, 360 (2015); https://doi.org/10.1016/j.cej.2015.06.044
56. F.C. Tsai, Y. Xia, N. Ma, J.J. Shi, T. Jiang, T.C. Chiang, Z.C. Zhang and W.C. Tsen, *Desal. Water Treat.*, **57**, 3218 (2016); https://doi.org/10.1080/19443994.2014.982199
57. S. Lin, Z. Song, G. Che, A. Ren, P. Li, C. Liu and J. Zhang, *Micropor. Mesopor. Mater.*, **193**, 27 (2014); https://doi.org/10.1016/j.micromeso.2014.03.004
58. S. Yoon, J.J. Calvo and M.C. So, *Crystals*, **9**, 17 (2019); https://doi.org/10.3390/cryst9010017
59. A.N. Ebelegi, N. Ayawei and D. Wankasi, *Open J. Phys. Chem.*, **10**, 166 (2020); https://doi.org/10.4236/ojpc.2020.103010
60. W.J. Weber and J.C. Morris, *J. Sanit. Engrg. Div.*, **89**, 31 (1963); https://doi.org/10.1061/JSEDAI.0000430
61. J. Wang and X. Guo, *Chemos.*, **309**, 136735 (2022); https://doi.org/10.1016/j.chemosphere.2022.136735